

ORIGINAL ARTICLE

Optimum Utilisation of CuO Nanofluid in Flat Plate Solar Collector

Nang Khin Chaw Sint, I.A. Choudhury* and H.H. Masjuki

Department of Mechanical Engineering, Faculty of Engineering, University of Malaya, 50603 Kuala Lumpur, Malaysia
Phone: +60163704658; Fax: +60379675317

ABSTRACT – The optimum utilisation of CuO-nanofluid in flat plate solar collector has been investigated under Malaysian climatic condition. To determine the optimum nanoparticle concentration required in the base fluid, a simulation was carried out using MATLAB program. From the simulation, it was found that, 0.5 vol.% of CuO nanoparticles in the base fluid yielded maximum collector efficiency. The test was conducted over six months following the ASHRAE standard with nanofluid in the flat plate collector to ascertain its efficiency. The maximum average solar radiation incident on the collector, collector outlet and ambient temperatures were observed about 1000 W/m², 50 °C and 38 °C respectively. From the efficiency curve, the absorbed and removed energy parameters were found to be 0.501 and 24.23 respectively. At a mass flow rate of one litre per minute, the maximum average instantaneous efficiency was 51%. The result of experimental efficiency was compared with the result of simulation and the efficiency values were within 4% of each other. CuO nanofluid based collector increases the efficiency compared to water as the collector fluid. The experimental results revealed that the efficiency of FPSC with CuO nanofluid was 4.78% higher than water base collector at the same mass flow rate of 1 L/min. The uncertainty analysis of result has shown that instantaneous efficiency uncertainty was about 3.3%. The simulation result has indeed minimised number of experiments required to determine the optimum concentration of nanofluid for maximum efficiency.

ARTICLE HISTORY

Received: 18th Aug 2020

Revised: 24th Oct 2020

Accepted: 13th Nov 2020

KEYWORDS

Nanofluid;

Optimum concentration;

Flat plate solar collector;

Instantaneous efficiency

NOMENCLATURE

A_c	surface area of the collector (m ²)	$T_o(t)$	collector outlet fluid temperature at time t (°C)
C_p	specific heat of the nanofluid (J/kg.K)	$T_{o,in}$	collector outlet fluid initial temperature (°C)
F_R	heat removal factor	U_L	heat loss coefficient (W/mK)
$F_R U_L$	removed energy parameter	$F_R(\tau\alpha)$	absorbed energy parameter
G_T	global solar radiation (W/m ²)	ΔT	temperature difference (°C)
m	mass flow rate of the nanofluid (kg.s ⁻¹)	u	uncertainty
R^2	correlation coefficient	$\tau\alpha$	effective-transmittance-absorptance product
T_a	ambient air temperature (°C)	η	instantaneous efficiency (%)
T_i	collector inlet fluid temperature (°C)	ϕ	nanofluid volume concentration (vol. %)
T_o	collector outlet fluid temperature (°C)		

INTRODUCTION

Renewable energy is the cleanest source of energy where proper and efficient use of it can prevent global warming by reducing carbon dioxide emissions. The conventional energy source, on the other hand, has a limited reserve and will be exhausted with time, and the use of this source leads to carbon dioxide emissions. The renewable energy source, although a viable option, has some limitations with regard to the cost of technologies [1-3]. Solar energy, as one of the abundantly available renewable energy resources, is the most gifted because it can be converted to heat and electricity. However, their use is limited because of low thermal efficiency [4]. The use of nanofluids in heat transfer devices can improve thermal performance.

Nanofluids consist of a base fluid and nanoparticles (1-100 nm) suspended within the base fluid. Nanoparticles usually metals or metal oxides have better thermal conductivities. The metallic nanoparticles are usually aluminium (Al), copper (Cu), and iron (Fe) while the metallic oxide nanoparticles are copper oxide (CuO), titanium dioxide (TiO₂), alumina (Al₂O₃), titanium dioxide (TiO₂) and silicon dioxide (SiO₂). These nanofluids have been utilised in many research areas such as in heat exchanger system, microchannel/fin system of cooling electronic devices, machining process in the manufacturing system, cold storage system, and cooling system in the car radiator for the enhancement of the heat transfer process and the development of the nanofluids [5-13]. Also, these nanofluids can be utilised solar collectors to enhance the thermal performance of the solar collector [14].

Flat plate solar collector, primarily the liquid type of solar collector, absorbs irradiation and transforms it into heat. The collector tubes containing the working fluid absorb the heat of radiation [15]. The current conventional working fluids for flat plate solar collectors have inherently poor heat transfer properties which limit the effectiveness of the heat transfer process in the collector [16-18]. This results in poor heat transfer between the absorber plate and heat transfer medium, resulting in the reduction of collector performance. In order to maximise the collector efficiency, the heat transfer loss to the working fluid must be minimised. One of the solutions is to use collector fluids, having better heat transfer characteristics. Recently, nanofluid is considered to be a better alternative having a great potential for heat transfer characteristic [19-20].

It has been reported in the literature that the efficiency of direct absorption solar collector with Al-H₂O working fluid was about ten per cent higher than that of the water-based collector. Also, the absorption of incident solar radiation by nanofluid was more than nine times than that of pure water-based collector [21]. The efficiency of a 10-110 MW solar collector increased when Therminol VP1/Graphite nanofluid was used [22]. An enhancement of 30% in the thermal performance of evaporator and evaporating with the application of CuO nanofluid in evacuated tubular solar collector was observed and compared to the water-based collector by researchers [23]. The efficiency of the parabolic solar collector using nanofluid of (Aluminium-Therminol VP-1) having 0.05% of volume concentration increased by 5%-10% [24]. Mojtaba et al. [25] conducted an experimental study to explore the effect of replacing water with TiO₂-water nanofluid in a symmetric flat plate collector (FPC). They found that the use of TiO₂-water nanofluids in place of water improved the efficiency of the collector. They reported maximum efficiency gains of 17.4%, 27.1%, and 33.5% for 1 wt.%, 3 wt.%, and 5 wt.% nanoparticle concentration respectively, compared to the water-filled collector. Yijie Tong [26] investigated the performance of FPC by water, Al₂O₃ nanofluid, and CuO nanofluid as the working fluids. According to their findings, the collector with Al₂O₃ nanofluid achieved the highest efficiency compared to the water-based collector (21.9 % higher). Experimental results showed that the use of Al₂O₃ and CuO nanofluids in the flat-plate solar collector could improve the thermal efficiency compared to the use of water, and the maximum performance of the flat-plate solar collector was obtained when 1.0 vol.-%-Al₂O₃ nanofluid used. Ali Jabari et al. [27] studied the effect of CuO-water nanofluid as the working fluid on the performance and the efficiency of a flat-plate solar collector experimentally. Their results revealed that utilising the nanofluid increased collector efficiency compared to water as an absorbing medium. The nanofluid with a mass flow rate of 1 kg/min increased the collector efficiency by 21.8%. For any particular working fluid, there was an optimum mass flow rate which maximised the collector efficiency. Sundar et al. [28] investigated the use of Al₂O₃/water nanofluids on the effectiveness of solar flat-plate collectors with and without twisted tape inserts experimentally. Their results of the heat transfer experiments indicated that for a Reynolds number of 13000, the heat transfer enhancement for 0.3% volume concentration of nanofluid was 21% for the plain tube and it was further enhanced to 49.75% when a twisted tape of H/D = 5 was inserted in the tube. Under the same operating conditions, the nanofluids/twisted tape inserts collector outperformed that with water and no twisted tapes. Sundar et al. [29] also studied the effectiveness of solar flat plate collector with Al₂O₃ water nanofluids and with longitudinal strip inserts. They conducted the experiments in the Reynolds number range from 5000 to 13,500, longitudinal strip inserts of aspect ratios equal to 1, 1.5 and 3, volume concentrations of 0.1% and 0.3%. From the results, it was observed that the Nusselt number enhancement for 0.3% volume concentration of nanofluid was 8.53% and 20.9% at Reynolds number of 5000 and 13,500, respectively compared with water data.

From the literature, it is apparent that nanofluid clearly enhances the heat transfer process. However, the heat transfer effectiveness mainly varies with the parameters of nanofluid (especially the volume concentration). Therefore, the selection of a proper nanofluid loading with optimum particle size and concentration for each particular application is the first priority. Optimisation of nanofluid parameters for nanofluid preparation becomes important. This can lead to not only minimising nanofluid preparation time and cost but also maximising heat transfer characteristics. Although there are many articles available on the theoretical and experimental investigation on the improvement of solar collector performance using nanofluids, very limited reports are available on optimising nanofluid used in solar collector application till now.

In light of the information from the current literature, the purpose of the present study is to determine the optimum concentration of CuO nanoparticles in the collector fluid that will result in the maximum collector efficiency. The optimum concentration of CuO-nanofluid has been determined by simulation under Malaysian climatic condition. In this investigation, firstly, a simulation was carried out using MATLAB program for various parametric conditions to optimise CuO nanofluid parameters (particle concentration and size). The simulation result was the basis for minimum experimentation necessary to determine the collector efficiency. Secondly, the CuO nanofluid was prepared using deionised water and CuO nanoparticles at optimal parameters and used as a collector fluid. The collector efficiency validation was done by conducting experiments in line with the guidelines of the ASHRAE 2003 standard. Finally, an uncertainty analysis was conducted to estimate the uncertainty in collector efficiency.

METHODOLOGY OF INVESTIGATION

Simulation

The solar collector thermal efficiency is evaluated by MATLAB program based-computer simulation using a set of equations incorporated in the MATLAB programmes. The details of these parametric equations, process and procedure of simulation are given in the article published by us [30]. The governing equations are given in Appendix A.

Firstly, the convective heat transfer coefficient (h_{fi}) of water-based CuO nanofluid as the working fluid was ascertained in evaluating the efficiency of the collector. The convective heat transfer coefficient was estimated from the Nusselt number of nanofluids as a function of size and volume concentration of nanoparticle. The overall heat loss factor (U_L) of the collector tilted at the optimum angle was estimated. Once the coefficients were obtained, they were used to compute the solar collector efficiency.

The nanoparticle size ($20 \text{ nm} < d_p < 150 \text{ nm}$) and volume concentration ($0 < \phi_p < 4 \%$) were considered as input variables in evaluating thermo-physical properties of H₂O-CuO nanofluid. These properties are the density (ρ_{nf}), viscosity (μ_{nf}), thermal conductivity (k_{nf}) and specific heat capacity ($c_{p,nf}$).

Experimental Setup and Procedure

Nanofluid preparation

The spherical-shape CuO nanoparticles (40 nm average diameter, 6.4 g/cm³ density) supplied by NovaScientific Resource, Malaysia with 99% purity were used for nanofluid preparation. The deionised water was used as a base fluid, and no surfactant was used for the dispersion of 0.5% volume CuO nanoparticle in the deionised water. A two-step method was used in preparing nanofluid, followed by continuous magnetic stirring for eight to ten hours in Fisher Scientific magnetic stirrer to guarantee even dispersion of nanoparticles in the deionised water. Afterwards, sonication was performed for one hour using Vibra-Cell VCX750 Ultrasonic processor to crash the agglomerations and bundles into smaller pieces.

Then the solution was left for one day, and the stability of nanofluid was visually analysed. No particle sedimentation was observed even after day one. After the second day, slight sedimentation was noticeable, but the suspension was not completely transparent. The prepared solution thus was a stable fluid with uniform thermo-physical fluid properties remaining constant throughout the fluid sample with respect to time. The copper oxide nanoparticles appeared as black powder while the nanofluid appeared as dark brownish to black colour.

The reason for using only 0.5% volume concentration is that the authors conducted a simulation analysis using MATLAB environment to determine the optimum volume concentration for CuO in the nanofluid. This concentration is obtained as the optimum for minimum overall heat loss coefficient (4.3 W/m²C) and maximum collector efficiency (54%) under Malaysian climatic condition. This is explained more in the Simulation Results section.

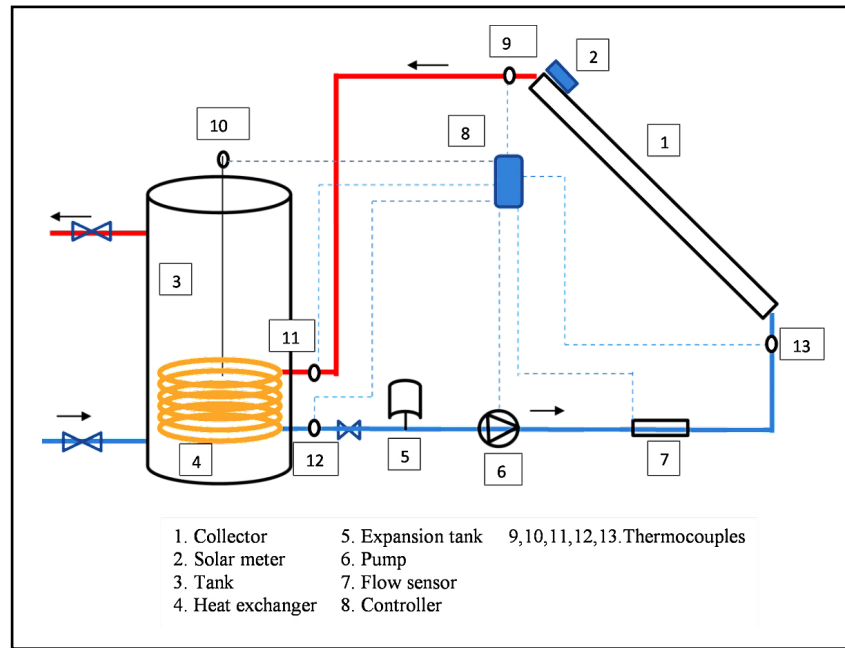
Experiments

The experimental setup was fabricated on the rooftop of a building located at the Faculty of Engineering, University of Malaya, Kuala Lumpur, Malaysia (latitude is 3°7'N and longitude is 101° 32'E) as shown in Figure 1(a). The solar collector used for the experiment was mounted south-facing at tilt-angle of 30°. This angle is the average optimum angle of the year for the fixed mounted collector. The incoming solar radiation received on the fixed collector surface was measured from September to February. The specification of the collector is presented in Table 1, and the diagram of the experimental test setup is shown in Figure 1(b). The area of the solar collector was 2 m² with eight collector tubes of 10 mm inside diameter and 2000 mm length.

The experimental setup consisted of a 100-litre water tank equipped with a heat exchanger (copper coil of tubing wraps around inside the perimeter of the tank) used to transfer the heat energy from the working fluid coming from the collector to the domestic water in the tank. The apparatus used during the test and their measurement accuracies are listed in Table 2. Five k-type thermocouples were used to monitor temperatures at the inlet of the tank (11), in the tank (10), at the outlet of the tank (12), at the inlet (13) and outlet of the collector (9). All thermocouples were connected to the digital display temperature indicators to monitor and record the temperatures. A TES 1333R solar meter was used to record total solar radiation on the collector. The wind speed was measured by a PROVA anemometer. A flow sensor (7) was used to measure the mass flow rate of nanofluid in the collector.



(a)



(b)

Figure 1. (a) Flat plate solar collector installed at the rooftop and, (b) the schematic of the experimental setup.

Table 1. Specification of the flat plate solar collector.

Specification	Dimension	Unit
Collector size	2000 × 1000 × 80	mm × mm × mm
Aperture area	1.84	m ²
Weight	35	Kg
Header tube size	22 × 0.6	mm × mm
Riser tube size	10 × 0.5	mm × mm
Solar absorption	95	%
Thermal emission	11	%

Table 2. Measurement accuracy of the apparatus.

Apparatus	Measurement accuracy
Thermocouples	± 0.1 °C
Solar radiation meter	± 10 W/m ²
Flow sensor	± 0.005 L/min
PROVA anemometer	± 0.1 m/s or ± 3.0%)

Test procedure

To ascertain the collector time-constant, after the steady-state condition was maintained, the collector was shielded from the receiving insolation, and the fluid temperatures at the collector inlet and outlet were observed immediately as a function of time until the steady-state temperature was reached. The collector time constant is the time needed for the fluid temperature at the collector outlet to reach 63.2% of its final steady-state value after a step change in insolation incident on the collector [31]. The response equation is in the following form:

$$\frac{T_o(t) - T_i}{T_{o,in} - T_i} = e^{-t} = 0.368 \tag{1}$$

where $T_o(t)$ is the collector outlet fluid temperature (°C) at time t , $T_{o,in}$ is the collector outlet fluid initial temperature (°C), and T_i is the collector inlet fluid temperature (°C).

The efficiency tests were performed according to the guideline of the ASHRAE2003 standard during steady-state conditions for various inlet temperatures. The data measurements of global irradiance on the collector surface, inlet and ambient air temperature and fluid flow rate were collected and averaged for each test period to produce a set of instantaneous efficiency data points. The instantaneous efficiency equation is as follows:

$$\eta_i = \frac{Q_u}{A_c G_T} = \frac{m C_p (T_o - T_i)}{A_c G_T} = F_R (\tau \alpha) - F_R U_L \frac{(T_i - T_a)}{G_T} \tag{2}$$

where, (in the nanofluid) C_p is the specific heat (4110 J/kg.K), m is the mass flow rate (kg.s⁻¹), T_o is the temperature at the collector outlet (°C), and T_i is the temperature at the collector inlet (°C), T_a is the ambient air temperature (°C), A_c is the surface area of the collector (m²), F_R is the heat removal factor, τ_α is the effective-transmittance-absorptance product, and U_L is the heat loss coefficient (W/mK).

Uncertainty analysis of efficiency

The instantaneous collector efficiency given in Eq. (2), is dependent on the specific heat (C_p) and mass flow rate (m) of nanofluid, temperature difference ($T_o - T_i$), collector area (A_c), and solar radiation (G_T). The uncertainty in the efficiency depends on the uncertainty of each of these variables and can be written as $\eta_i = f(m, C_p, \Delta T, A_c, G_T)$. The uncertainty in η_i can be expressed as $u_{\eta_i} = f_1(u_m, u_{C_p}, u_{\Delta T}, u_{A_c}, u_{G_T})$. The propagation of uncertainty in the variables to the result yields an uncertainty estimate [32] given by:

$$u_{\eta_i} = \pm \left[(\theta_m u_m)^2 + (\theta_{C_p} u_{C_p})^2 + (\theta_{\Delta T} u_{\Delta T})^2 + (\theta_{A_c} u_{A_c})^2 + (\theta_{G_T} u_{G_T})^2 \right]^{0.5} \tag{3}$$

where, by referring to Eq. (2),

$$\theta_m = \frac{\partial \eta_i}{\partial m}, \theta_{C_p} = \frac{\partial \eta_i}{\partial C_p}, \theta_{\Delta T} = \frac{\partial \eta_i}{\partial \Delta T}, \theta_{A_c} = \frac{\partial \eta_i}{\partial A_c}, \theta_{G_T} = \frac{\partial \eta_i}{\partial G_T} \tag{4}$$

Dividing each of these derivatives by Eq. (2), the uncertainty Eq. (3) can be written as:

$$\frac{u_{\eta_i}}{\eta_i} = \pm \left[\left(\frac{\theta_m u_m}{\eta_i} \right)^2 + \left(\frac{\theta_{C_p} u_{C_p}}{\eta_i} \right)^2 + \left(\frac{\theta_{\Delta T} u_{\Delta T}}{\eta_i} \right)^2 + \left(\frac{\theta_{A_c} u_{A_c}}{\eta_i} \right)^2 + \left(\frac{\theta_{G_T} u_{G_T}}{\eta_i} \right)^2 \right]^{0.5} \tag{5}$$

Substituting the values of derivatives $\theta_m, \theta_{C_p}, \theta_{\Delta T}, \theta_{A_c}$, and θ_{G_T} into Eq. (5), the uncertainty in the efficiency can be written as:

$$\frac{u_{\eta_i}}{\eta_i} = \pm \left[\left(\frac{u_m}{m} \right)^2 + \left(\frac{u_{C_p}}{C_p} \right)^2 + \left(\frac{u_{\Delta T}}{\Delta T} \right)^2 + \left(-\frac{u_{A_c}}{A_c} \right)^2 + \left(-\frac{u_{G_T}}{G_T} \right)^2 \right]^{0.5} \tag{6}$$

RESULTS AND DISCUSSION

Simulation Results

The maximum hourly average total solar radiation was evaluated by Matlab code based on Duffie model [35] for six months (September to February) from 8:00 to 17:00 hours. The highest solar radiation obtained was in February (at 1.8 MJ/m² h), and the lowest was 1.16 MJ/m²h in December, as shown in Figure 2.

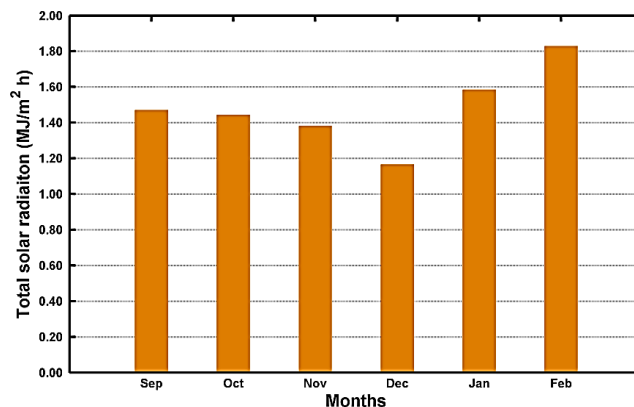


Figure 2. Maximum hourly average total solar radiation data on months (of September-February) from 8:00 to 17:00 hours.

The nanofluid density as a function of particle volume concentration for various nanoparticle diameters (25-120 nm) is shown in Figure 3. The density is observed to increase with the particle volume concentration. At 0.1 % nanoparticle volume concentration the density was 991 kg/m³ while that at 3.5 % volume concentration it was 1184 kg/m³. Figure 4 shows that the specific heat capacity of nanofluid decreases from 4143 to 3707 J/kg. K, as the particle volume concentration increases. It is due to the fact that metals have lower specific heat compared to liquids. Figure 5 shows the

thermal conductivity versus particle volume concentration at various particle sizes. As the particle volume concentration increases, the thermal conductivity of nanofluid increases due to a higher concentration of nanoparticle.

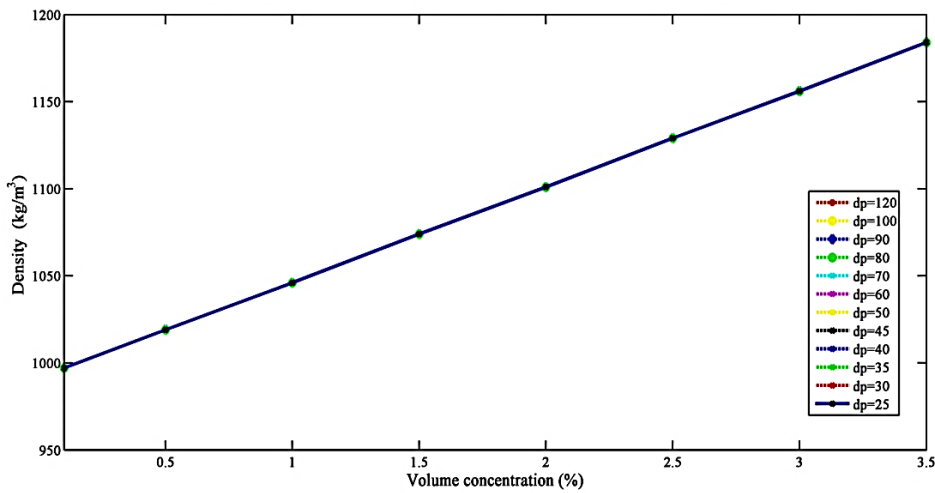


Figure 3. CuO nanofluid density as a function of the particle volume concentration at different particle diameters.

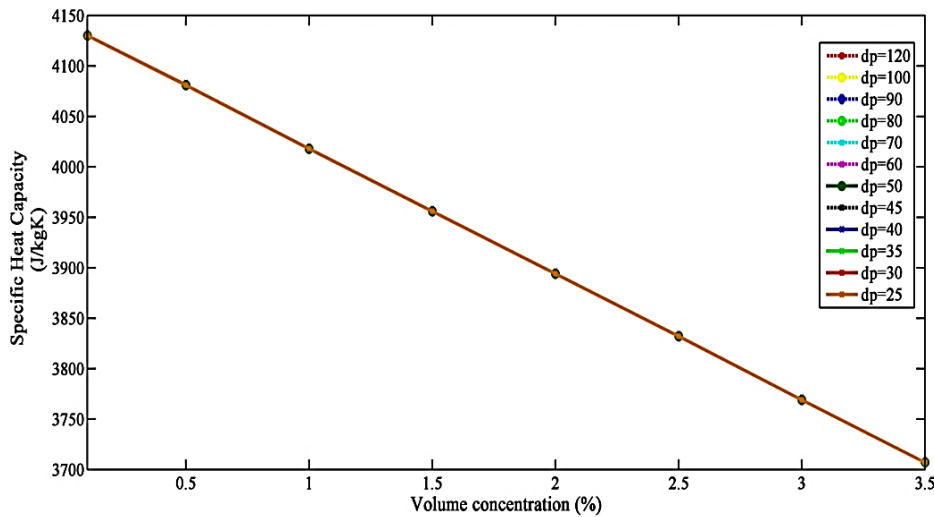


Figure 4. Specific heat capacity of copper oxide nanofluid as a function of particle volume concentration at different particle diameters.

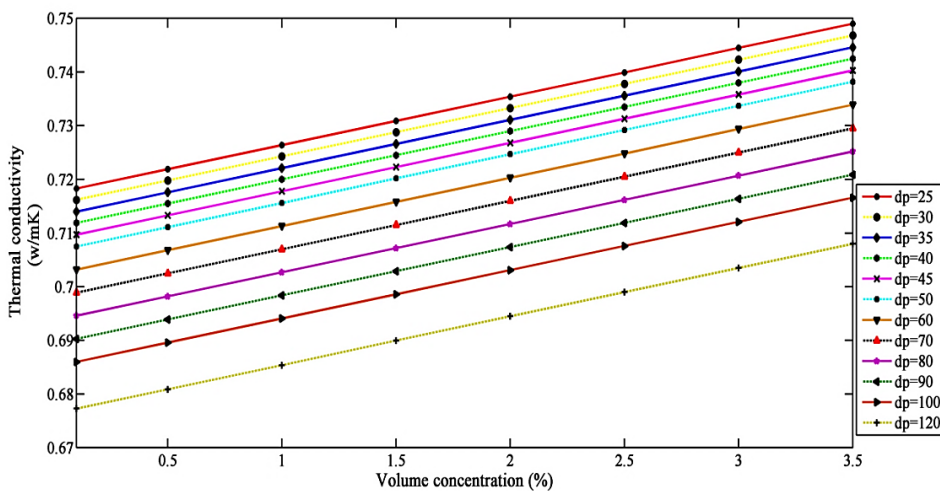


Figure 5. Thermal conductivity of copper oxide nanofluid as a function of particle volume concentration at various particle diameters.

However, the nanofluid thermal conductivity decreases with increasing nanoparticle sizes, and a similar trend was also observed in previous findings [5]. The figure shows that the thermal conductivity of 25 nm CuO nanofluid was the highest compared to all other higher diameters CuO nanofluid. It is believed, the smaller nanoparticles could form cluster type particles forming large interfacial areas between particles and liquid enhancing rate of the heat transfer process. Also, it could be due to the effect of nanoparticles sizes. The smaller nanoparticles in the fluid in suspension can induce micro-movement of nanoparticles initiating micro-convection between particles and liquid. The phenomenon can increase the heat transfer between the liquid (water) and nanoparticles. Consequently, the thermal conductivity increases more with smaller nanoparticles. There has been more than 15 % increase in the thermal conductivity of nanofluid when the particle diameter reduces from 120 nm to 40 nm at 2 % nanoparticle concentration.

Figure 6 shows that with the increase in nanoparticle volume concentration, viscosity increases. The viscosity is observed to increase as the diameter of nanoparticle diameter in the base water increases. It is noted that the viscosity is affected much more by the particle concentration than the particle diameter. The viscosity of 25 nm CuO nanofluid increased by 44 % when the particle volume concentration increases from 0.1 to 3.5% in the water-based fluid. The convective heat transfer coefficient, as shown in Figure 7, is observed to increase with the increase of nanoparticle volume concentration in the nanofluid for a specific particle diameter. The coefficient of heat transfer varies from 4026 w/m²K to 24277 w/m²K as the particle volume concentration increases from 0.1% to 3.5% for 25 nm CuO nanofluid. However, the coefficient of heat transfer was higher for smaller diameter particles. At the larger volume concentration of particles, the decrease in the coefficient of heat transfer is higher with increasing particle diameter. Hence, the heat transfer coefficient is strongly dependent on the volume concentration rather than the particle diameter. Figure 8 presents the coefficient of overall heat loss of the collector with nanoparticle volume concentration for various nanoparticle sizes. The minimum overall heat loss coefficient was found at 0.5% nanoparticle concentration. The thermal efficiency of the collector is presented in Figure 9. At a given collector design condition, the maximum efficiency was found to be 54 % at 0.5 vol.% CuO nanoparticle in the nanofluid.

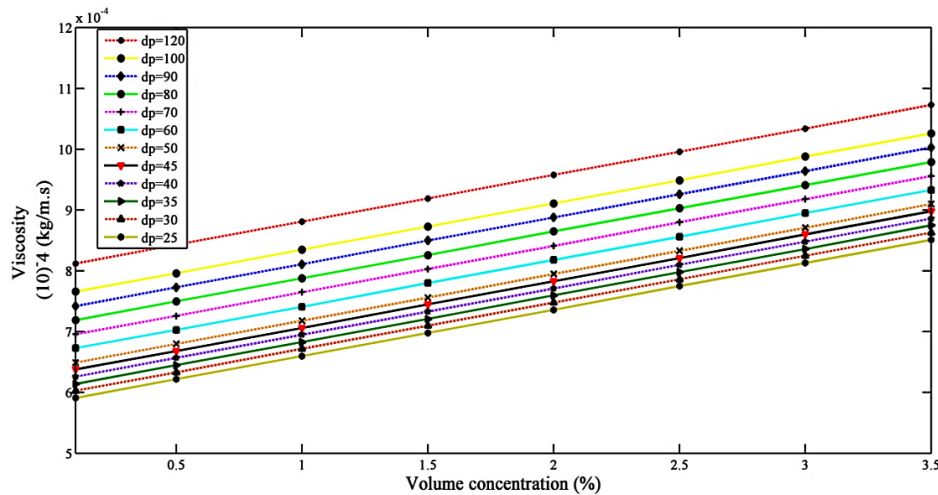


Figure 6. Variation of the viscosity of CuO-nanofluid with the particle volume concentration for different particle diameters.

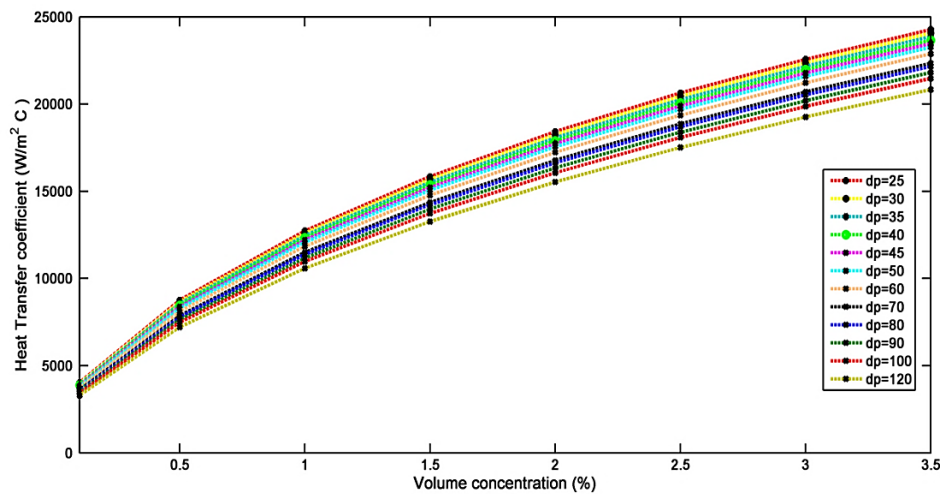


Figure 7. Coefficient of heat transfer of copper oxide nanofluid as a function of particle volume concentration at various nanoparticle diameters.

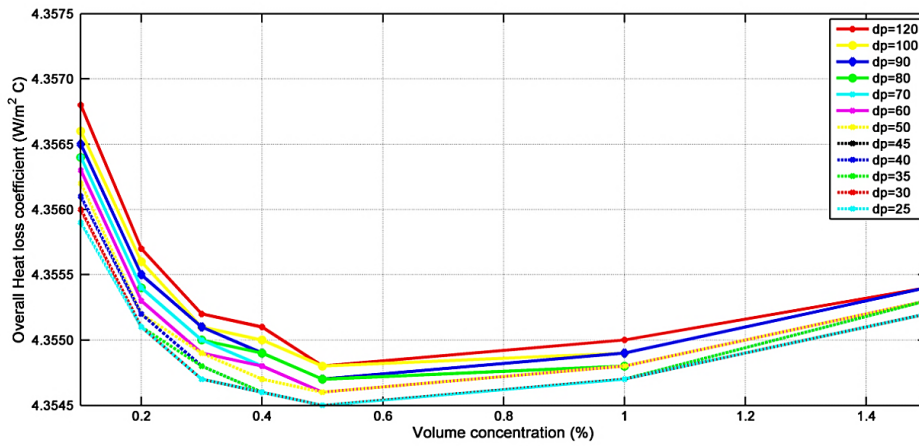


Figure 8. Minimum overall heat losses occurred at 0.5% particle concentration loading.

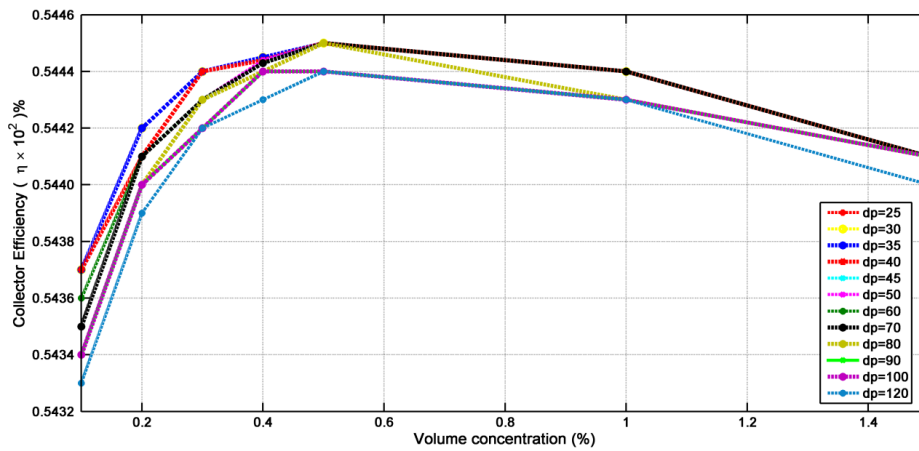


Figure 9. Collector efficiency at different nanoparticle volume concentrations loading.

Experimental Results

The variation of average total solar radiation from 11:00 to 15:00 hours for six months (September-February) is shown in Figure 10. The maximum hourly average total solar radiation was recorded in February (at 1.47 MJ/m²h), and the minimum was recorded in November (at 0.96 MJ/m²h).

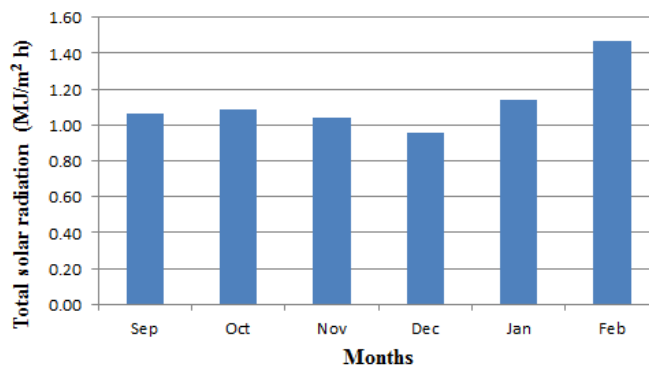


Figure 10. Maximum hourly average total solar radiation data on months (of September-February) from 11:00 to 15:00 hours.

Following the ASHRAE 2003 guidelines, the thermal performance of the collector was determined. The outdoor tests under standard steady-state condition have been carried out from 11:00 to 15:00 hours for several days of the months, according to the ASHRAE 2003 guidelines. The weather condition was mixed (rainy, cloudy, windy) during these test days. The data were collected every five minutes on the test days, which had a bright clear sky between the time intervals of 11:00 to 15:00 hours. Each test period for each test day was divided into 12-time intervals of 60 min (1 hr). So, there were data collected for several clear days. Therefore the average value was obtained for each test period (1hr). There was 4 tests period per test day since the time interval for each test day was from 11:00 to 15:00 hours. Then, this average value (12 values) for each test period (1 hr) has been reported as a single data point (12 points) for each test period (1 hr).

Figure 11 shows the experimental data were recorded over the test days. During the test, the mean global solar radiation fluctuated between 720 W/m² to 1100 W/m², the average ambient temperatures (T_a) between 32 °C and 38 °C, the mean inlet temperature (T_i) between 32 °C and 39 °C, and the average outlet temperature (T_o) between 33 °C and 50 °C. The time constant of the collector has been determined as per standard and were found to be 2.37 min for the mass flow rate of 1 L/min and 1.45 min for 2 L/min, respectively. This means that the collector requires 2.37 min to warm up and cool down with the sudden change in irradiation at one litre per minute flow rate and 1.45 min at 2 L/min mass flow rate. The mean data obtained for each test period is reported in the diagram to plot the efficiency curve for the fixed-mount flat plate solar collector. The efficiency curve is generated by applying a least-squares linear fit of the data points.

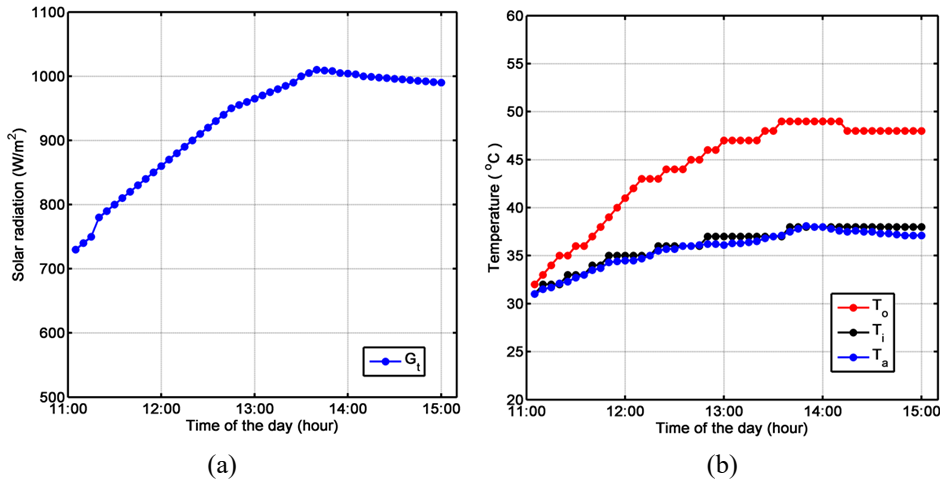


Figure 11. Experimental data on test days of (a) solar radiation, and (b) collector outlet temperature, T_o , collector inlet temperature, T_i and ambient temperature, T_a .

Figure 12 shows the experimental instantaneous efficiency versus $(T_i - T_a)/G_T$. The linear relation between η and $(T_i - T_a)/G_T$ is obtained at one litre and two litres per minute mass flow rate with R^2 values of 0.979 and 0.987, respectively. The efficiency equations for these two mass flow rates are:

$$\eta = 0.501 - 24.23(T_i - T_a) / G_T \tag{7}$$

$$\eta = 0.589 - 39.47(T_i - T_a) / G_T \tag{8}$$

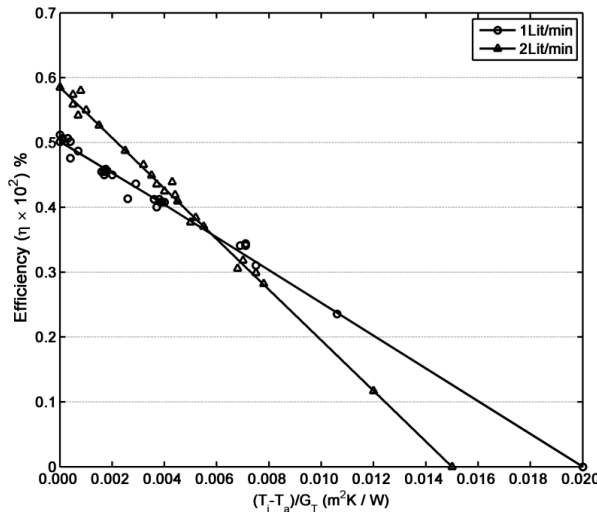


Figure 12. Efficiency of CuO nanofluid based flat plate solar collector for two flow rates.

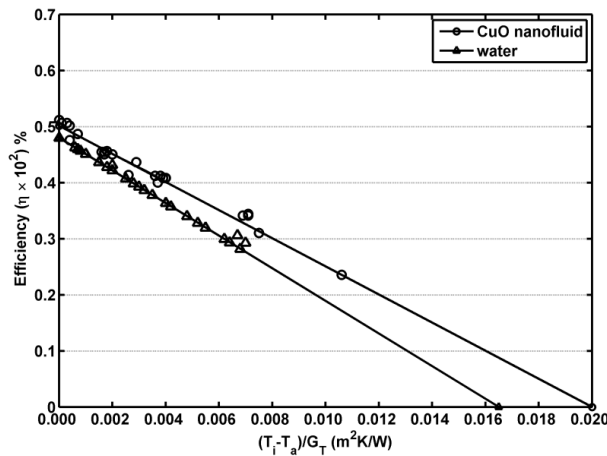


Figure 13. Collector efficiency with CuO nanofluid and water at one liter per minute.

It can be seen from Figure 12 that the collector efficiency was found to be the highest when the reduced temperature parameter $(T_i - T_a)/G_T$ was zero, and when the reduced temperature parameter was maximum, collector efficiency was zero. It was found that the efficiency decreases as $(T_i - T_a)/G_T$ increases. This could be due to the rise of either the solar radiation, G_T , or the difference between collector inlet temperature and ambient temperature or the heat loss alternately from the collector. The experimental value of absorbed energy parameter $F_R(\tau\alpha)$ was 0.501, and removed energy parameter $F_R U_L$ was 24.23 at the mass flow rate of 1 L/m. The values of $F_R(\tau\alpha)$ and $F_R U_L$ were 0.589 and 39.47, respectively, at the mass flow rate of 2 L/m. The maximum average instantaneous efficiency using 0.5 vol.% CuO nanofluid was observed to be about 50 % at one litre per minute flow rate and about 59 % at 2 L/m flow rate. From the results, it can be said that the collector efficiency is directly proportional to the Reynolds number. The results agree with the findings of researchers listed in reference [5]. However, the researchers [5] achieved higher efficiency, although the trend of the graph is very similar. As shown in Figure 13, the efficiency of FPSC with CuO nanofluid is higher than with water as collector fluid. The values of $F_R(\tau\alpha)$ and $F_R U_L$ for water in one litre per minute mass flow rate were observed to be 0.4773 and 27.71, respectively. A comparison of $F_R(\tau\alpha)$ and $F_R U_L$ value for CuO nanofluid and water at one litre per minute flow rate is presented in Table 3.

Table 3. Value of $F_R(\tau\alpha)$ and $F_R U_L$ for CuO nanofluid and water at litre per minute flow rate.

Fluid	Water	CuO Nanofluid (0.5% vol.)
$F_R(\tau\alpha)$	0.477	0.501
$F_R U_L$	27.71	24.23
R^2	0.986	0.979

According to various literature [33-34], the performance of solar collector with smaller nanoparticle is superior to that with a larger nanoparticle. The thermal conductivity of nanofluids is higher for smaller size nanoparticles. As the thermal conductivity of working fluids becomes higher, the heat transfer rate is enhanced and consequently, the efficiency increases. Table 4 shows comparative efficiency values obtained by simulation and experiment at the recommended mass flow rate of one litre per minute [35]. The experimental efficiency value is very close to the value obtained by simulation, and the results are within 4 % of each other.

Table 4. Experimental and theoretical efficiency of the collector at one litre per minute.

ϕ	Flow rate	η (simulation)	η (experimental)
CuO nanofluid (0.5% vol.)	1 L/min	54%	50%

Estimation of Uncertainty in Instantaneous Efficiency

Substituting the values of uncertainty in Eq (6),

$$\frac{u_{\eta_i}}{\eta_i} = \pm \left[\left(\frac{0.005}{1} \right)^2 + \left(\frac{20}{4110} \right)^2 + \left(\frac{0.1}{6} \right)^2 + \left(-\frac{0.05}{2} \right)^2 + \left(-\frac{10}{910} \right)^2 \right]^{0.5} \tag{9}$$

$$\frac{u_{\eta_i}}{\eta_i} = \pm 0.0327 = 3.27\%$$

By inspecting Eq. (9), it is clear that the last three items make practically the major contribution towards the uncertainty of the collector efficiency.

CONCLUSION

The conclusions are as follows:

- i. The simulation study prior to experimentation could be useful in saving experimental time and cost. In the present simulation, the optimum volume concentration of nanoparticles obtained was 0.5% for maximum collector efficiency. With this concentration as the basis, experimental validation was made through test data. There was no need for carrying experiments at a different volume concentration of nanoparticles.
- ii. Nanoparticles with smaller diameter are efficient in enhancing the heat transfer rate compared to larger particle diameter. The enhancement of the heat transfer coefficient is about 28% at 0.5% volume concentration when the particle diameter decreases from 120 nm to 40 nm
- iii. The experimental instantaneous efficiency of flat plate solar collector having copper oxide nanofluid as the working fluid has been determined under Malaysian weather condition. A linear relationship between the instantaneous efficiency and the reduced temperature is established for flow rates of 1 L/min and 2 L/min. The efficiency values were between 50% and 59%. The efficiency obtained from the experiment is compared with the simulation result at the flow rate of one litre per minute. It is found that the results obtained experimentally are within 4% of the simulation results from a quantitative point of view. The experimental results also showed that the efficiency of FPSC with CuO nanofluid was 4.78% higher than water base-collector at the same mass flow rate of 1 L/min.
- iv. The overall system uncertainty of instantaneous efficiency was about 3.3%. This was due to the contribution of various component uncertainties in the system like the specific heat and mass flow rate of nanofluid in the collector, the difference of collector outlet and inlet temperatures, collector area, and solar radiation. The specific heat and mass flow rate appeared to have a negligible effect on the overall uncertainty compared to the remaining components of Eq. (9).

ACKNOWLEDGEMENT

This research was supported by the Japan International Cooperation Agency (JICA) under the AUN/SEED-Net Collaborative Research with Industry (CRI) Program.

REFERENCES

- [1] Bellos E, Tzivanidis C, Moschos K. Antonopoulos, Energetic and financial evaluation of solar-assisted heat pump space heating systems. *Energy Conversion and Management* 2016; 120:306-319.
- [2] Wang K, He YL, Qiu Y, Zhang Y. A novel integrated simulation approach couples MCRT and Gebhart methods to simulate solar radiation transfer in a solar power tower system with a cavity receiver. *Renewable Energy* 2016; 89:93-107.
- [3] Gautam A, Chamoli S, Kumar A, Singh S. A review on technical improvements, economic feasibility and world scenario of solar water heating system. *Renewable and Sustainable Energy Review* 2017; 68, 1:541–562.
- [4] Bellos E, Korres D, Tzivanidis C, Antonopoulos KA. Design, simulation and optimisation of a compound parabolic collector. *Sustainable Energy Technology and Assessments* 2016; 16: 53–63.
- [5] Razak NFD, Sani MSM, Azmi WH, Heat transfer augmentation in heat exchanger by using nanofluids and vibration excitation - A review. *International Journal of Automotive and Mechanical Engineering* 2019; 17:7719-7733.
- [6] Venkatadri K, Abdul Gaffar S, Prasad VR, Hidayathualla Khan BM, Beg OA, Simulation of natural convection heat transfer in a 2-D trapezoidal enclosure. *International Journal of Automotive and Mechanical Engineering* 2019; 16: 7375-7390.
- [7] Srinu Gugulothu, Vamsi Krishna Pasam, Performance evaluation of CNT/MoS₂ hybrid nanofluid in machining for surface roughness. *International Journal of Automotive and Mechanical Engineering* 2019; 16: 7413-7429.
- [8] Ting TW, Hung YM, Osmam MS, Yeki PNY, Heat and flow characteristics of nanofluid flow in porous microchannels. *International Journal of Automotive and Mechanical Engineering* 2019; 15; 5238-5250.
- [9] Ferrouillat S, Bontemps A, Poncelent O, Soriano O, Gruss JA. Influence of nanoparticle shape factor on convective heat transfer and energetic performance of water-based SiO₂ and ZnO nanofluids. *Applied Thermal Engineering* 2013; 55:839- 851.
- [10] Ham J, Kim J, Cho H. Theoretical analysis of thermal performance in a plate-type liquid heat exchanger using various nanofluids based on LiBr solution. *Applied Thermal Engineering* 2016; 108:1020-1032.
- [11] He QB, Wang SF, Tong MW, Liu YD. Experimental study on thermo- physical properties of nanofluids as phase-change material (PCM) in low temperature cool storage. *Energy Conversion and Management* 2012; 64:199-205.
- [12] Peyghambarzadeh SM, Hashemabadi SH, Naraki M, Vermahmoudi Y. Experimental study of overall heat transfer coefficient in the application of dilute nanofluids in the car radiator. *Appl. Therm. Eng* 2013; 52: 8-16.
- [13] Kole M, Dey TK. Thermal performance of screen mesh wick heat pipes using water-based copper nanofluids. *Appl. Therm. Eng* 2013; 50:763-770.
- [14] He QB, Zeng S, Wang SF. Experimental investigation on the efficiency of flat plate solar collectors with nanofluids. *Applied Thermal Engineering* 2015; 88:165–171.

- [15] Alvarez A, Cabeza O, Muñi MC, Varela LM. Experimental and numerical investigation of a flat-plate solar collector. *Energy* 2010; 35:3707-3716.
- [16] Layek A, Saini JS, Solanki SC, Second law optimisation of a solar air heater having chamfered rib–groove roughness on absorber plate. *Renewable Energy* 2007; 32(12): 1967–1980.
- [17] Trisaksri V, Wongwises S, Critical review of heat transfer characteristics of nanofluids. *Renewable and Sustainable Energy Review* 2007; 11: 512-523.
- [18] Santhi N. Enhancement of heat transfer by nanofluids in solar collectors. *International Journal of Innovations in Engineering and Technology (IJET)* 2014; 3 (4): 2319-1058.
- [19] Lee S, Choi. SUS. Application of metallic nanoparticle suspensions in advanced cooling systems. In: Kwon Y, Davis D, Chung H., editors. *Recent advances in solids/structures and application of metallic materials*, New York: ASME, 1996, p 227-234.
- [20] Chandrasekar M, Suresh S, Chandra Bose A. Experimental investigations and theoretical determination of thermal conductivity and viscosity of Al₂O₃/water nanofluid. *Experimental Thermal and Fluid Science* 2010; 34: 210-216.
- [21] Tyagi H, Phelan P, Prasher R. Predicted efficiency of a low-temperature nanofluid based direct absorption solar collector. *Journal of Solar Energy Engineering* 2009; 131 041004.
- [22] Taylor RA, Phelan PE, Otanicar TP, Walker CA, Nguyen M, Trimble S. Prasher R. Applicability of nanofluids in high flux solar collectors, *Journal of Renewable and Sustainable Energy* 2011; 3: 023104.
- [23] Lu L, Liu ZH, Xiao HS, Thermal performance of an open thermosyphon using nanofluids for high-temperature evacuated tubular solar collectors, Part 1: Indoor experiment. *Solar Energy* 2011; 85: 379-87.
- [24] Khullar V, Tyagi H, Phelan PE, Otanicar TP, Singh H, Taylor RA. Solar energy harvesting using a nanofluids-based concentrating solar collector. In: *Proceedings of MNHMT2012 3rd Micro/Nanoscale. Heat and Mass Transfer International Conference Atlanta, USA; 3–6 March, 2012.*
- [25] Mojtaba MM, Vahabzadeh B, Yu G, Larry K.B.L, Doranehgard MH, Kun H, Qingang X, Enhancing the efficiency of a symmetric flat-plate solar collector via the use of rutile TiO₂-water nanofluids, *Sustainable Energy and Technology Assessments* 2020; 40: 100783.
- [26] Yijie T, Hoseong L, Woobin K, Honghyun C, Energy and exergy comparison of a flat-plate solar collector using water, Al₂O₃ nanofluid, and CuO nanofluid, *Applied Thermal Engineering* 2019; 159: 113959.
- [27] Ali Jabari M, Mahmood FG, Mahmood S, Monireh HZ, Effects of CuO/water nanofluid on the efficiency of a flat-plate solar collector, *Experimental Thermal Fluid Science* 2014; 58: 9-14.
- [28] Sundar LS, Singh MK, Punnaiah V, Sousa ACM, Experimental investigation of Al₂O₃/water nanofluids on the effectiveness of solar flat-plate collectors with and without twisted tape inserts, *Renewable Energy* 2018; 119: 820-833.
- [29] Sundar LS, Kirubeil A, Punnaiah V, Sousa ACM, Effectiveness analysis of solar flat plate collector with Al₂O₃ water nanofluids and with longitudinal strip inserts, *International Journal of Heat and Mass Transfer* 2018; 127: 422-435.
- [30] Nang Khin Chaw Sint, Choudhury IA, Masjuki HH, Aoyama H. Theoretical analysis to determine the efficiency of a CuO-water nanofluid based-flat plate solar collector for domestic solar water heating system in Myanmar. *Solar Energy* 2017; 155: 608-619.
- [31] Yousefi T, Veysi F, Shojaezadeh E, Zinadini S. An experimental investigation on the effect of Al₂O₃–H₂O nanofluid on the efficiency of flat-plate solar collectors, *Renewable Energy* 2012; 39: 293-298.
- [32] Figliola RS, Beasley DE. *Theory and design for mechanical measurements*, fourth ed., (Asia) Pte Ltd: John Wiley & Sons; 2006.
- [33] Jang PS, Choi SUS. Effects of various parameters on nanofluid thermal conductivity. *Journal of Heat Transfer* 2007; 129: 617.
- [34] Palabiyik I, Musina Z, Witharana S, Ding Y. Dispersion stability and thermal conductivity of propylene glycol-based nanofluids. *Journal of Nanoparticles Research* 2011; 13: 5049-5055.
- [35] Duffie A, Beckman WA. *Solar engineering of the thermal processes*. fourth ed., New York: JohN Wiley and Sons; 2013.

APPENDIX A

Governing equations [30].

Heat transfer coefficient:

$$h_{fi} = \frac{Nu k}{D_i} \tag{A.1}$$

Nusselt number:

$$Nu_{nf} = 0.4328 (1 + 11.285 \phi_p^{0.754} Pe_d^{0.218}) Re_{nf}^{0.333} Pr_{nf}^{0.4} \text{ (laminar)} \tag{A.2}$$

$$Nu_{nf} = 0.0059 (1.0 + 7.6286 \phi_p^{0.6886} Pe_d^{0.001}) Re_{nf}^{0.9238} Pr_{nf}^{0.4} \text{ ((turbulent))} \tag{A.3}$$

Reynolds number:

$$Re = \frac{4\dot{m}}{\pi \mu_{fn} D} \tag{A.4}$$

Peclet number:

$$Pe_d = \frac{4\dot{m}_p C_{pnf}}{\pi D^2 k_{nf}} \quad (\text{A. 5})$$

Viscosity:

$$\mu_{nf} = \mu_w \left(0.9042 + 0.1245\phi_p - 0.08445 \left[\frac{T_{nf}}{72} \right] + 0.6436 \left[\frac{d_p}{170} \right] \right) \quad (\text{A. 6})$$

Thermal conductivity:

$$k_{nf} = k_w \left(0.9808 + 0.0142\phi_p + 0.2718 \left[\frac{T_{nf}}{70} \right] - 0.1020 \left[\frac{d_p}{150} \right] \right) \quad (\text{A. 7})$$

Specific heat capacity:

$$C_{pnf} = C_{pw} \left(1.036 - 0.0298\phi_p - 0.07261 \left[\frac{T_{nf}}{70} \right] \right) \quad (\text{A. 8})$$

Overall heat loss coefficient:

$$U_L = U_t + U_b + U_e \quad (\text{A. 9})$$

Efficiency factor:

$$F' = \frac{1/U_L}{W \left(\frac{1}{U_L [D + (W - D)F]} \right) + \frac{1}{C_b} + \frac{1}{\pi D h_{fi}}} \quad (\text{A. 10})$$

Heat remover factor:

$$F_R = \frac{\dot{m}C_p}{A_c U_L} \left[1 - \exp \left(- \frac{A_c U_L F'}{\dot{m}C_p} \right) \right] \quad (\text{A. 11})$$

Total solar radiation:

$$I_T = I_b R_b + I_d \left(\frac{1 + \cos \beta}{2} \right) + I_{\rho_g} \left(\frac{1 - \cos \beta}{2} \right) \quad (\text{A. 12})$$